HOXA13 regulates the expression of bone morphogenetic proteins 2 and 7 to control distal limb morphogenesis

Wendy M. Knosp[2,*], Virginia Scott[1,*], Hans Peter Bächinger[1,3] and H. Scott Stadler[1,2,†]

[1]Shriners Hospital for Children, Research Division, Portland, Oregon 97239, USA
[2]Department of Molecular and Medical Genetics, Oregon Health and Science University, Portland, Oregon 97239, USA
[3]Department of Biochemistry and Molecular Biology, Oregon Health and Science University, Portland, Oregon 97239, USA
*These authors contributed equally to this work
†Author for correspondence (e-mail: hss@shcc.org)

Accepted 24 June 2004

Development 131, 4581-4592
Published by The Company of Biologists 2004
doi:10.1242/dev.01327

Summary

In humans and mice, loss of HOXA13 function causes defects in the growth and patterning of the digits and interdigital tissues. Analysis of *Hoxa13* expression reveals a pattern of localization overlapping with sites of reduced *Bmp2* and *Bmp7* expression in *Hoxa13* mutant limbs. Biochemical analyses identified a novel series of *Bmp2* and *Bmp7* enhancer regions that directly interact with the HOXA13 DNA-binding domain and activate gene expression in the presence of HOXA13. Immunoprecipitation of HOXA13-*Bmp2* and HOXA13-*Bmp7* enhancer complexes from the developing autopod confirm that endogenous HOXA13 associates with these regions. Exogenous application of BMP2 or BMP7 partially rescues the *Hoxa13* mutant limb phenotype, suggesting that decreased BMP signaling contributes to the malformations present in these tissues. Together, these results provide conclusive evidence that HOXA13 regulates *Bmp2* and *Bmp7* expression, providing a mechanistic link between HOXA13, its target genes and the specific developmental processes affected by loss of HOXA13 function.

Key words: HOXA13, BMP2, BMP7, Limb, Apoptosis, Gene regulation

Introduction

The analysis of limb development has yielded remarkable insights into the molecular and genetic mechanisms required to form a functional three-dimensional structure. In mice, initiation of the forelimb buds occurs at embryonic day (E) 9.0 as a small outgrowth of the lateral plate mesoderm at the junction of the caudal and thoracic somites (Tickle et al., 1976; Solursh et al., 1990; Kaufman and Bard, 1999). Following induction, limb bud growth and expansion continues under the influence of signals emanating from the three primary limb axes, including: FGFs to maintain proliferation in the proximodistal axis; sonic hedgehog, which establishes the zone of polarizing activity in the anteroposterior axis; and *Wnt7a* and *En1*, which specify the dorsoventral polarity of the developing limb (Riddle et al., 1993; Parr and McMahon, 1995; Chiang et al., 1996; Crossley et al., 1996; Ohuchi et al., 1997; Loomis et al., 1998; Min et al., 1998; Sekine et al., 1999; Lewandoski et al., 2000; Moon and Capecchi, 2000).

Although many of the genes required for normal limb development have been identified (for reviews, see Niswander, 2003; Mariani and Martin, 2003; Logan, 2003; Gurrieri et al., 2002; Tickle, 2003), surprisingly little is known about how these genes are transcriptionally regulated. Among the factors likely to regulate the expression of limb patterning genes are the 5′ HOX transcription factors, whose loss-of-function phenotypes demonstrate their capacity to regulate key developmental processes such as cell adhesion, apoptosis, proliferation and migration (Dollé et al., 1989; Davis and Capecchi, 1994; Davis et al., 1995; Fromental-Ramain et al., 1996a; Fromental-Ramain et al., 1996b; Stadler et al., 2001; Wellik and Capecchi, 2003; Boulet and Capecchi, 2004; Spitz et al., 2003; Kmita et al., 2002). Although it is clear that HOX proteins mediate many of the cellular events during limb morphogenesis, the mechanistic links between these transcription factors, their target genes, and their effects on specific cellular processes are still largely unknown (Stadler et al., 2001; Morgan et al., 2003; Wellik and Capecchi, 2003; Boulet and Capecchi, 2004). One reason for this is that HOX proteins may not regulate the global expression of any particular target gene, but instead control the development of specific tissues through direct interactions with tissue-specific gene regulatory elements (Hombría and Lovegrove, 2003; Grenier and Carroll, 2000; Weatherbee et al., 1998).

In the developing limb, HOXA13 localizes to discrete domains within the interdigital and interarticular regions, where its function is required for interdigital programmed cell death (IPCD), digit outgrowth and chondrogenesis (Stadler et al., 2001; Fromental-Ramain et al., 1996a). This observation led us to hypothesize that HOXA13 directly regulates genes whose products are necessary for IPCD and joint formation. Testing this hypothesis, we detected changes in the expression of the genes encoding bone morphogenetic proteins 2 and 7 (*Bmp2*, *Bmp7*) in the interdigital and distal joint tissues, suggesting that HOXA13 may directly regulate their expression in these discrete regions. Scanning the DNA sequences upstream of *Bmp2* and *Bmp7*, we identified a series

of nucleotide sequences preferentially bound by the HOXA13 DNA-binding domain (A13-DBD). In vitro characterization of these DNA sequences revealed they function as enhancer elements that, in the presence of HOXA13, activate the expression of reporter constructs, independent of sequence orientation. Furthermore, in the developing autopod, endogenous HOXA13 binds these same enhancer elements, which can be immunoprecipitated with a HOXA13-specific antibody. In *Hoxa13* mutant limbs, both IPCD and *Msx2* expression are partially restored with exogenous BMP2 or BMP7 treatment, suggesting that HOXA13 is required for sufficient levels of BMP2 and BMP7 to be expressed in the interdigital tissues, as well as for these tissues to fully respond to BMP signaling. Together, these results provide the first molecular evidence that HOXA13 controls distal limb morphogenesis through the direct regulation of *Bmp2* and *Bmp7* expression, whose combined functions are necessary for normal digit morphogenesis and IPCD.

Materials and methods

Mouse strains

Hoxa13 homozygous mutant mice were produced by heterozygous mutant intercrosses, using the previously described *Hoxa13*^{GFP} mutant allele and genotyping procedures (Stadler et al., 2001). *Bmp7* mutant embryos were produced by intercrosses of heterozygous mutant *Bmp7* mice (Jackson Laboratories, Bar Harbor, ME). The *Bmp7* mutant allele was originally described by Luo et al. (Luo et al., 1995). Embryo genotypes were determined by using PCR with primers specific for the PGK-HPRT disruption present in the mutant *Bmp7* allele and with DNA derived from the embryo yolk sac. All care and analysis of *Hoxa13*^{GFP} and *Bmp7* mice was carried out in accordance with an approved mouse handling protocol.

RNA in situ hybridization and immunohistochemistry

Antisense riboprobes specific for *Bmp2*, *Bmp4* and *Bmp7* were generated using plasmids kindly provided by B. Hogan (*Bmp2* and *Bmp4*; Duke University, NC) and R. Beddington (*Bmp7*; NIMR, London), whereas *Hoxa13*, *Msx2*, and BMP-receptor *IA*, *IB* and *II* riboprobes were produced as described (Morgan et al., 2003). Whole mount in situ hybridization, immunohistochemistry and confocal imaging of limb frozen sections were performed as described by Manley and Capecchi, and by Morgan et al. (Manley and Capecchi, 1995; Morgan et al., 2003). Antibodies to BMP2/4 (AF355) and BMP7 (AF354) were purchased from R&D Systems, and were used at 0.02 μg/ml on frozen limb sections.

Analysis of programmed cell death

TUNEL analysis was performed as described by Stadler et al. (Stadler et al., 2001). Limbs from E13.5 *Hoxa13* and *Bmp7* wild-type, heterozygous- and homozygous-mutant embryos were examined using a Bio-Rad MRC 1024 confocal laser imaging system fitted with a Leica DMRB microscope. Images were produced by compiling z-series scans of the intact limb buds, typically averaging 40-50 sections at 1 μm per section. Kalman Digital Noise reduction was used for all samples.

Limb organ culture and BMP supplementation

Affi-gel blue beads (Bio-Rad) washed five times in sterile PBS were incubated at 4°C overnight in solutions containing 0.1 mg/ml of rhBMP2 (R&D Systems) or rhBMP7 (R&D Systems), or in sterile PBS. Beads were inserted into the interdigital mesenchyme of E13.5 wild-type, heterozygous- and homozygous-mutant limbs between digits II and III, and III and IV. Limb explants containing the beads were placed on 0.4 μm HTTP Isopore membrane filters (Millipore), coated with gelatin in 60 mm organ culture dishes (Falcon), and grown in BGJb media (Invitrogen), supplemented with 50% rat whole-embryo culture serum (Harlan Bioproducts), 50 U/ml penicillin and 50 μg/ml streptomycin, for 8 hours in an incubator at 37°C, 10% CO_2. The limb explants were examined for induced *Msx2* expression or for changes in programmed cell death, using TUNEL analysis of frozen sections as described (Morgan et al., 2003).

Synthesis and structural characterization of the HOXA13 DNA-binding domain

Protein synthesis and purification

The 67 amino acid HOXA13 DNA-binding domain (A13-DBD) (GRKKRVPYTKVQLKELEREYATNKFITKDKRRRISATTNLSER QVTIWFQNRRVKEKKVINKLKTTS) was synthesized on an ABI 443A peptide synthesizer (Applied Biosystems, Foster City, CA), using Fmoc-Ser(tBu)-PEG-PS resin (PerSeptive Biosystems, 0.16 mmol/g) and Fmoc amino acids (Anaspec). After synthesis, the peptide was purified to greater than 95% purity, using a Gilson Model 321 High Performance Liquid Chromatography (HPLC) system fitted with a semi-preparative reversed-phase peptide column (Grace Vydac, C18, 15 μm, 300 Å, 250×25 mm). The mass and purity of the A13-DBD peptide was verified using a Micromass time-of-flight mass spectrometer (Q-tof micro, Waters, Manchester, UK), peptide sequencing and amino acid analysis.

Circular dichroism spectroscopy

The thermal stability and folding of the A13-DBD peptide into a helix-turn-helix DNA-binding motif was verified by circular dichroism (CD). The A13-DBD peptide was reconstituted to a final concentration of 100 μM in 50 mM NaF (buffered to pH 7.2 with phosphate buffer). CD spectra were obtained using an Aviv 202 spectropolarimeter and a 0.1 mm path length rectangular cell (Hellma, Müllheim, Germany). The wavelength spectra represent at least an average of 10 scans with 0.1 nm wavelength steps. Thermal transitions were recorded at a heating rate of 10°C/hour in a 1 mm cell.

DNA-binding site identification with the HOXA13 DNA-binding domain

The A13-DBD peptide was solubilized to a concentration of 500 nM in PBS, and incubated with radioactively labeled *Bmp2* and *Bmp7* upstream regions (200-300 base pair fragments) at 4°C in gel shift buffer (Promega). 5′ upstream sequences for *Bmp2* and *Bmp7*, representing nucleotides –600 to +1 for *Bmp2* (Ensembl ref: ENSMUSG00000027358), and –3113 to +1 for *Bmp7* (Ensembl ref: ENSMUSG00000008999), were examined for binding by the A13-DBD peptide, using electrophoretic mobility shift assays (EMSA) on a 4% non-denaturing polyacrylamide gel buffered with 0.5×TBE. PCR fragments exhibiting reduced electrophoretic mobility in the presence of the A13-DBD peptide were subdivided into 30-50 base-pair (bp) regions and synthesized as self-annealing oligonucleotides (Oligos Etc, Wilsonville, OR) to narrow the regions bound by HOXA13. Double-stranded oligonucleotides were prepared by heating 1 μM oligonucleotide stock solutions in 50 mM Tris-HCl (pH 7.2), 50 mM NaCl to 95°C for 5 minutes and allowing them to cool to room temperature. Annealed oligonucleotides (12 nM) were radiolabeled using terminal transferase and α^{32}P-ddATP (5000 Ci/mmol) (Amersham), as described by the manufacturer (Roche). Peptide concentrations and EMSA assay conditions were the same as described, with the exception that 6% polyacrylamide 0.5×TBE gels were used to resolve the protein-DNA complexes.

Sequences of the self-annealing oligonucleotides

BMP7C1, TTGACTGAGAGATAATGGGGTGGAAGGAGCCCCT-CCTTCCACCCCATTATCTCTCAGTCAA;

*BMP2*C1, ATTTAGTTAATTGCAGGTTCAAGAAGCCCCTTCT-TGAACCTGCAATTAACTAAAT;

*BMP2*C3, TTGTGTCTGTTAATATGCACATGAGCGAGCCCCT-CGCTCATGTGCATATTAACAGACACAA; and

*BMP2*C4, CTTTTTAATTGGGAGTTAAGAAGCCCCTTCTTAA-CTCCCAATTAAAAAG.

Cell culture and luciferase assays

Luciferase plasmid constructs

DNA regions bound by the A13-DBD peptide were amplified from mouse genomic DNA by using PCR and the following primers:

BMP2, 5′-ATTTAGTTAATTGCAGGAAGGT-3′ and 5′-ACTCC-CAATTAAAAAGAGCATT-3′; and

BMP7s1, 5′-GGAAGTGCAGAAGCACCC-3′ and 5′-ATGGTA-ATCACTCAGACCTAA-3′.

PCR conditions used a 2 minute soak at 94°C, followed by 35 cycles of 94°C, 54°C and 72°C for 30 seconds each step. Amplified PCR products were cloned in both orientations into the *Sma*I site of the pGL3 luciferase vector (Promega) to produce the pGL3BMP2FLuc, pGL3BMP2RLuc, pGL3BMP7FLuc and pGL3BMP7RLuc plasmids. The sequences and orientation of the cloned fragments were verified using di-deoxy terminator fluorescent sequencing.

Hoxa13-HA expression plasmid

The *Hoxa13*-HA expression plasmid (pCMV-A13) used in the luciferase and immunoprecipitation assays was produced using a 2-kb genomic region containing the murine *Hoxa13* locus. An HA epitope tag was added to the 3′ end of the *Hoxa13* coding region, using a unique *Spe*I restriction site to add the following annealed oligonucleotides:

5′-CTAGTGGAGGATACCCATACGACGTCCCAGACTACGCT-TAAGATATCA-3′; and

5′-CTAGTGATATCTTAAGCGTAGTCTGGGACGTCGTATGGG-TATCCTCCA-3′.

Cell culture and transfection

NG108-15 cells were grown as recommended by the supplier (ATCC). At 90% confluence, the cells were passaged into 12-well dishes (Costar), grown at 37°C, 10% CO_2 for 24 hours, and then transfected with 2 μg of pGL3BMP2 or pGL3BMP7, 2 μg of pCMV-A13, or 2 μg of empty pCMV vector, and 0.5 μg of the pRL-CMV Renilla plasmid (Promega) to normalize for transfection efficiency. All transfections used the Superfect Reagent, as recommended by the manufacturer (Qiagen). Forty-eight hours after transfection, cells were rinsed with PBS, lyzed with M-Per lysis reagent (Pierce), and processed to detect luciferase activity using the Dual-Glo Luciferase Assay System (Promega). Luciferase activity was determined as the average of three separate readings of each well (1 second/read), using a Packard Fusion Universal Microplate Analyzer (Perkin Elmer). For each experimental condition four separate transfections were performed. Results were normalized for transfection efficiency using relative Renilla luciferase expression levels, as described by the manufacturer (Promega), and plotted using SigmaPlot 8.0 (SPSS).

Hoxa13 antibody production

A HOXA13 peptide, corresponding to amino acids 1-43 of the murine HOXA13 (MTASVLLHPRWIEPTVMFLYDNGGGLVADELNKN-MEGAAAAAA) (Mortlock and Innis, 1997) was used to immunize New Zealand White rabbits. Samples exhibiting high *Hoxa13* antibody titers by ELISA were assessed for specificity to the full-length HOXA13, using western blot and immunohistochemistry of cultured limb mesenchyme derived from mice heterozygous for a temperature-sensitive T-antigen (Immorto® mice, Charles River Laboratories) and homozygous for the HOXA13-GFP mutant allele. A Cytological Nuclear Stain Kit (Molecular Probes) was used to label nuclei with DAPI.

Chromatin immunoprecipitation (ChIP)

ChIP assays were performed using a chromatin immunoprecipitation assay, as described (Upstate Biotechnology), with the following modifications: limb buds from E12.5 *Hoxa13*^{GFP} wild-type and homozygous-mutant embryos were dissected in PBS containing 15 μl/ml protease inhibitor cocktail (PIC) (Sigma). Lysates were sonicated for four periods of 10 seconds at 4°C using a Microson (Misonix) sonicater at 15% output. To avoid sample heating, tubes were placed in an ice/EtOH bath for 5 seconds before and after each sonication. Cell lysates were pre-cleared with 80 μl Gammabind (Amersham) containing 40 μg/ml tRNA (Roche) in 10 mM Tris-HCl (pH 8), 1 mM EDTA (GBS). After pre-clearing, all centrifugation steps were performed at 100 ***g*** for 2 minutes. Fifteen microliters of *Hoxa13* antibody or control solution (PBS) were used at the immunoprecipitation step. For collection of *Hoxa13* antibody/HOXA13/DNA complexes, 60 μl of GBS was added to the samples. The Gammabind/*Hoxa13* antibody/HOXA13/DNA complexes were washed twice for 5 minutes at 4°C for each wash step. DNA was eluted from the immune complexes by digesting overnight at 45°C in 50 mM Tris-HCl (pH 8.4), 1 mM EDTA, 0.5% Tween-20 containing 20 μg/ml Proteinase K (Invitrogen). Eluted DNA from the antibody or no antibody control samples were assessed for the presence of the *Bmp2*, *Bmp7s1* or *Bmp7s2* DNA regions using PCR and the primers described above. For *Bmp7s2*, the following primers were used to PCR amplify immunoprecipitated chromatin: 5′-GCCTCTGTTCT-TGCTGCGCT-3′ and 5′-ACATGAACATGGGCGCCG-3′.

Results

Hoxa13 is expressed in discrete regions of the developing autopod

Examination of *Hoxa13* expression in the developing autopods revealed a dynamic spatiotemporal pattern of expression in tissues critical for IPCD and digit chondrogenesis. At E12.5 *Hoxa13* expression is localized to the distal autopod mesenchyme in both the digit condensations and interdigital tissues (data not shown) (Haack and Gruss, 1993). By E13.5 *Hoxa13* expression transfers to the peridigital tissues and interarticular condensations (Fig. 1A), whereas in E14.5 forelimbs, *Hoxa13* expression becomes restricted to the distal interarticular joint fields and nail beds (Fig. 1C). In homozygous mutants, the localization of *Hoxa13* transcripts is consistently elevated at all gestational ages when compared with wild-type controls, suggesting either that HOXA13 may negatively regulate its own expression or that mutant *Hoxa13-GFP* transcripts turn over at a slower rate than wild-type *Hoxa13* mRNA (Fig. 1B,D).

To correlate the sites of *Hoxa13* localization with malformations present in *Hoxa13* mutant limbs, we examined digit separation and development in E15.5 limbs. In these tissues, the loss of *Hoxa13* function resulted in severe malformations of the distal joints, as well as a persistence of the interdigital tissues (Fig. 1E,F) (Stadler et al., 2001; Fromental-Ramain et al., 1996a). Interestingly, the separation of digits II-V is effected in a highly reproducible pattern in *Hoxa13* mutant forelimbs, where digits II-III and IV-V exhibit the greatest degree of soft-tissue fusion, whereas digits III-IV exhibit modest removal of the distal interdigital tissue (Fig. 1C-F).

Reduced *Bmp2* and *Bmp7* expression in *Hoxa13* mutant autopods

Recognizing that limbs lacking *Hoxa13* exhibit severe defects in the initiation of IPCD and joint formation (Stadler et al., 2001) (Fig. 1), and that BMP2 and BMP7 function as key regulators of IPCD and digit chondrogenesis (Zuzarte-Luís and

Hurlé, 2002; Merino et al., 1998; Macias et al., 1997; Zou et al., 1997; Yokouchi et al., 1996; Zou and Niswander, 1996), we examined their expression in *Hoxa13* wild-type and mutant forelimbs. Analysis of *Bmp7* expression in E12.5-13.5 wild-type embryos revealed high levels of expression in the interdigital tissues (Fig. 1G,I). By contrast, age-matched homozygous mutants exhibited a marked reduction in *Bmp7* expression in the interdigital and peridigital regions, specifically in domains that co-express *Hoxa13* (Fig. 1H,J,S-V).

Bmp2 expression was also reduced in the interdigital tissues, the developing nail beds, and the distal joints of E12.5 and E14.5 homozygous mutants, which exhibited a diffuse distribution of *Bmp2* transcripts when compared with wild-type controls (Fig. 1A,C,K-N). Next, to determine whether the loss of BMP signaling in *Hoxa13* mutant limbs affects the expression of BMP-regulated genes, we examined *Msx2* expression in the distal interdigital tissues. In *Hoxa13* mutant limbs, *Msx2* expression was noticeably reduced in the

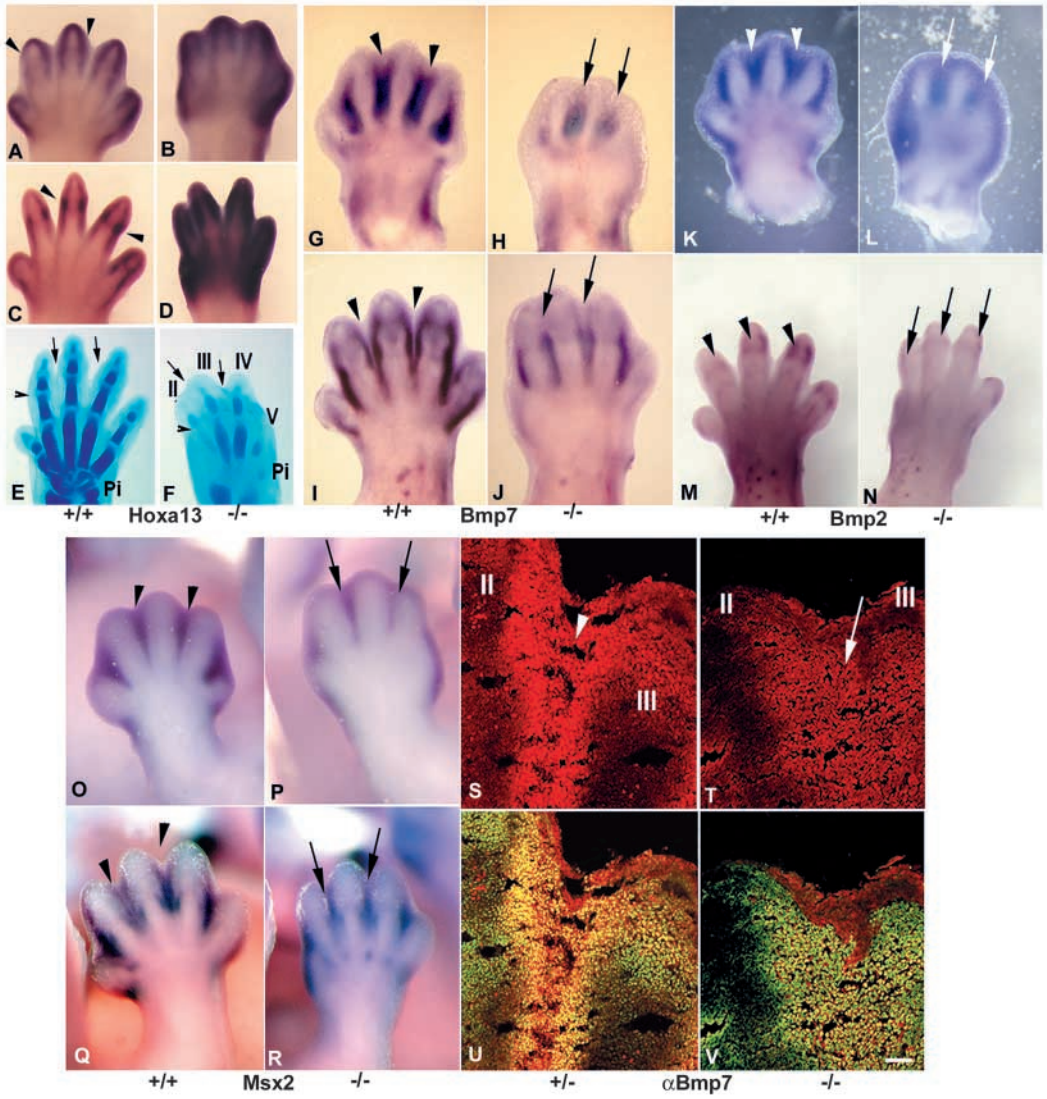

Fig. 1. Spatiotemporal expression of *Hoxa13* correlates with sites of malformation and decreased BMP expression. (A-D) Analysis of *Hoxa13* expression by in situ hybridization using an exon 1-specific riboprobe. *Hoxa13* expression is present in the distal interdigital mesenchyme and peridigital tissues (A, arrowheads). (C) Hoxa13 localizes to the distal joint/nail bed in E14.5 limbs (arrowheads). (B,D) In homozygous mutants, elevated levels of *Hoxa13* exon 1 transcripts were detected throughout the autopod. (E,F) Alcian Blue staining of E15.5 mutant limbs reveals defects in distal digit separation (F, arrows) and chondrogenesis (arrowheads), when compared with wild-type controls. Pi, pisiform carpal element. (G-J) *Bmp7* expression is reduced (arrows) in the distal interdigital tissues at E12.5 (G,H) and in the peridigital tissues at E13.5 (I,J) of homozygous *Hoxa13* mutants, when compared with age-matched wild-type controls (arrowheads). (K-N) *Bmp2* expression is reduced (arrows) in the interdigital tissues of E12.5 *Hoxa13* mutant embryos, and in the distal joints/nail beds of E14.5 *Hoxa13* mutants, when compared with wild-type controls (arrowheads). (O-R) *Msx2*, a target of BMP signaling, exhibits reduced interdigital expression in E12.5-E13.5 mutant limbs (arrows) compared with age-matched controls (arrowheads). (S,U) BMP7 (red, arrowhead) and HOXA13-GFP (green) co-localize (yellow cells in U and V) in the interdigital tissues of E12.5 limbs. (T,V) Age-matched homozygous mutants exhibit reduced numbers of BMP7-positive cells in the same interdigital regions (arrow), a finding consistent with the reduced *Bmp7* transcripts in these same tissues (compare H and T). Scale bar: 50 μm.

interdigital tissues when compared with wild-type controls at E12.5 and E13.5 (Fig. 1O-R).

To verify that BMP7 and HOXA13 proteins co-localize to the same cells in developing interdigital tissues, we examined BMP7 and HOXA13 protein distribution using a BMP7 antibody and the HOXA13-GFP fusion protein. In E12.5 autopods, HOXA13-GFP and BMP7 proteins co-localized to the same cells in the distal interdigital tissues of both heterozygous and homozygous mutants (Fig. 1S-V). However, the interdigital tissues of *Hoxa13* homozygous mutants consistently exhibited fewer BMP7-positive cells, as predicted by the decreased levels of *Bmp7* transcripts in this region (Fig. 1H,J). Co-localization of HOXA13-GFP and BMP2 proteins could not be determined by immunohistochemistry because commercially available BMP2 antibodies failed to detect BMP2 protein in autopod frozen sections at E12.5 or E13.5 (data not shown).

HOXA13 directly binds DNA regions upstream of *Bmp2* and *Bmp7*

Because *Bmp2*, *Bmp7* and *Hoxa13* are co-expressed in the developing limb, and their expression is reduced in *Hoxa13* mutants, we hypothesized that HOXA13 may directly regulate *Bmp2* and *Bmp7* expression in the distal autopod. To address this possibility, a HOXA13 DNA-binding domain peptide (A13-DBD) was used to screen DNA regions upstream of *Bmp2* and *Bmp7* for direct HOXA13 binding. Prior to this analysis, it was necessary to confirm that the putative DNA-binding domain present in the C terminus of HOXA13 actually folds into a DNA-binding structure and to determine the

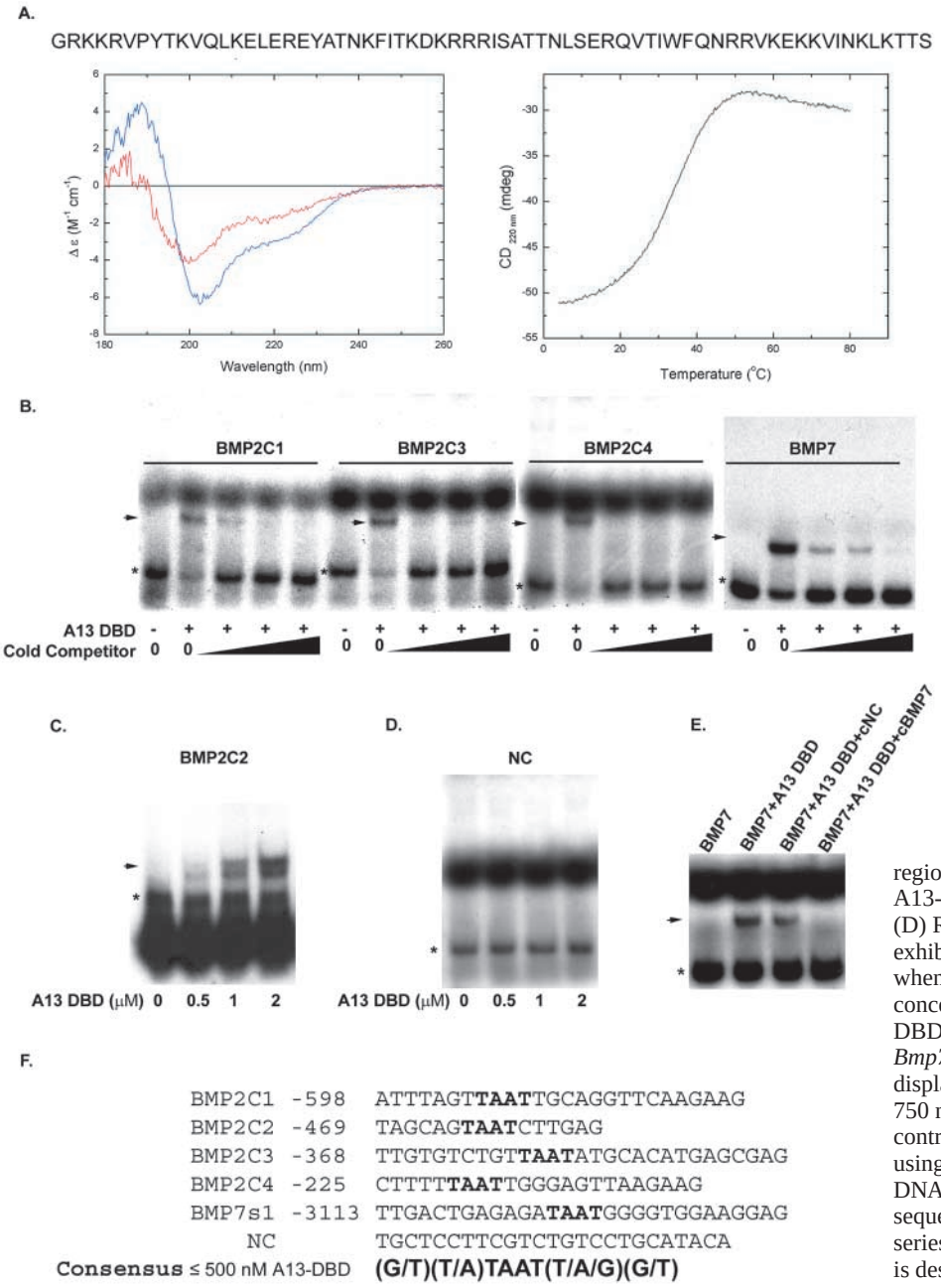

Fig. 2. Structural and functional analysis of the HOXA13 DNA-binding domain. (A) The amino acid sequence of the A13-DBD peptide is presented above. (Left panel) Structural analysis of the A13-DBD peptide by circular dichroism spectroscopy indicates that the peptide folds into a stable α-helical DNA-binding motif at 4°C (blue curve). At 60°C, the majority of the α-helical content is lost by thermal denaturation (red curve). (Right panel) Thermal stability measurements of the A13-DBD peptide showed that the α-helical conformation is maintained between 4 and 25°C. At temperatures higher than 25°C, the peptide cooperatively transforms to its denatured conformation. (B-E) A13-DBD peptide exhibits specific binding for the DNA regions present upstream of *Bmp2* and *Bmp7*. Asterisks denote unbound radiolabeled DNA, arrowheads denote A13-DBD-DNA complexes (B,C,E). (B) Quantitation of the A13-DBD affinity for the bound DNA regions using increasing concentrations (black triangles) of cold competitor DNA (0, 150, 300 and 750 nM) revealed differential A13-DBD affinities for each of the bound sites. (C) The *Bmp2C2* region requires 2-fold greater concentrations of A13-DBD to affect its electrophoretic mobility. (D) Radiolabeled control DNA sequences exhibited no change in electrophoretic mobility when incubated with 4-fold (2 μM) higher concentrations of the A13-DBD peptide. (E) A13-DBD binding specificity was confirmed using the *Bmp7C1* binding site, which could not be displaced from the A13-DBD peptide by using 750 nM concentrations of the unlabeled negative control DNA (cNC), but is completely displaced using 750 nM unlabeled *Bmp7C1* competitor DNA (cBMP7C1). (F) Analysis of the DNA sequences bound by the A13-DBD reveals a novel series of HOX binding sites. The core TAAT site is designated in bold type.

biophysical conditions that maintain proper folding for subsequent DNA-binding studies.

Characterization of the A13-DBD secondary structure by circular dichroic spectroscopy (CD) revealed the peptide stably folds into an α-helical structure, consistent with the predicted helix-turn-helix DNA-binding motif encoded by the A13-DBD peptide (Fig. 2A, left panel). The folded A13-DBD peptide also exhibited reasonable thermal stability, maintaining its α-helical structure between 4 and 25°C (Fig. 3A, right panel). At temperatures higher than 25°C, the A13-DBD peptide showed a cooperative transition to a denatured conformation (Fig. 2A, right panel), confirming that the majority of the A13-DBD peptide folds into the detected α-helical motif. Based on this analysis, we performed our DNA-binding experiments at temperatures between 4 and 25°C in order to maintain A13-DBD secondary structure stability. By contrast, full-length HOXA13 could not be examined for proper folding and function, as the molecule prepared by in vitro translation was only soluble in a denatured state, preventing CD analysis, as well as its use as a DNA-binding molecule (data not shown).

To identify HOXA13 binding sites upstream of *Bmp2* and *Bmp7*, the A13-DBD peptide was incubated with 200- to 400-base pair (bp) regions upstream of *Bmp2* and *Bmp7*. In the presence of the A13-DBD peptide, strong DNA binding was detected within 600 bp of the *Bmp2* initiation codon, whereas for *Bmp7* an A13-DBD binding site was not detected until 3000 bp upstream of the initiation codon (data not shown). Using self-annealing oligonucleotides, the minimal DNA sequences bound by the A13-DBD peptide were identified (Fig. 2B). Within the *Bmp2* upstream region, four A13-DBD binding sites, *Bmp2 C1-C4*, were identified. For the bound *Bmp7* upstream region, a single A13-DBD binding site, *Bmp7C1*, was identified (Fig. 2B). Competition experiments revealed that the A13-DBD peptide exhibited specificity and differential affinity for each of the bound DNA sequences (Fig. 2B,C). For *Bmp2*, the A13-DBD peptide exhibited the highest affinity for regions C1 and C3, which required competitor DNA concentrations of between 300 and 750 nM to displace the bound radiolabeled probe. By contrast, the A13-DBD peptide exhibited less affinity for *Bmp2* region C4, where 150 nM concentrations of competitor DNA were sufficient to completely displace the corresponding radiolabeled oligonucleotide (Fig. 2B). A fourth *Bmp2* DNA region, *Bmp2*C2, was also bound by the A13-DBD peptide; however, 2- to 4-fold higher concentrations of A13-DBD were required to affect its electrophoretic mobility (Fig. 2C).

Analysis of the *Bmp7C1* binding site revealed the highest A13-DBD affinity for any of the A13-DBD bound sequences, requiring competitor DNA concentrations of greater than 750 nM to completely displace the radiolabeled *BMP7C1* oligonucleotide (Fig. 2B,E). The DNA-binding specificity of A13-DBD was confirmed using a randomized self-annealing oligonucleotide that exhibited no changes in electrophoretic mobility in the presence of 4-fold higher concentrations of A13-DBD peptide (Fig. 2D). Similarly, concentrations of control oligonucleotide greater than 750 nM could not displace the A13-DBD-bound *Bmp7C1* oligonucleotide, confirming high affinity and specificity for the *Bmp7C1* binding site (Fig. 2E).

Analysis of the DNA sequences bound by the A13-DBD peptide revealed a HOX-specific TAAT nucleotide core sequence (Fig. 2F). However the nucleotides flanking the TAAT site varied greatly from sequences bound by other HOX proteins, suggesting that HOXA13 may recognize unique DNA sequences to facilitate its tissue-specific regulation of gene expression (Catron et al., 1993; Pellerin et al., 1994). Interestingly, a second TAAT-containing region (*Bmp7s2*) was identified in the sequences upstream of *Bmp7*; however, in the presence of the A13-DBD peptide the *Bmp7s2* sequence did not exhibit any change in electrophoretic mobility (data not shown), suggesting that nucleotides flanking the TAAT core sequence in *Bmp7s1* confer binding specificity.

The *Bmp2* and *Bmp7* sequences bound by A13-DBD function as enhancers of gene expression in vitro

A 384 bp fragment containing the four *Bmp2* binding sites (BMP2C1-C4) was cloned into a luciferase reporter plasmid and tested for in vitro transcriptional regulation by HOXA13. Cells transfected with the *Bmp2* luciferase vector and the *Hoxa13* expression plasmid (pCMV-A13) exhibited a consistent increase in relative luciferase activity (RLA) when compared with control transfections lacking pCMV-A13 (Fig. 3A). Comparisons of forward and reverse orientations of the 384 bp upstream region revealed a 2.5- and 1.8-fold increase in RLA, suggesting that the 384 bp *Bmp2* region functions as a HOXA13-regulated enhancer of gene expression (Fig. 3A,C). Similarly, a 216 bp fragment containing the BMP7C1-binding site also caused an increase in luciferase reporter expression, resulting in a 1.8- and 2.0-fold increase in RLA for the forward and reverse orientations, respectively (Fig. 3B,C). Our detection of direct interactions between A13-DBD and these enhancer elements, as well as the ability of these enhancer elements to drive reporter gene expression only in the presence of HOXA13 strongly supports our hypothesis that HOXA13 directly regulates the expression of *Bmp2* and *Bmp7* in the developing autopod.

HOXA13 associates with the *Bmp2* and *Bmp7* enhancer elements in the developing autopod

To verify that HOXA13 also binds the *Bmp2* and *Bmp7* enhancer regions in vivo, a *Hoxa13* antibody was developed to immunoprecipitate endogenous HOXA13-DNA complexes from limb bud chromatin. To identify both wild-type and mutant HOXA13 proteins, the *Hoxa13* antibody (αHoxa13) was raised against the N-terminal region of HOXA13, which is conserved in both wild-type and mutant protein isoforms. Analysis of the proteins recognized by αHoxa13 revealed two predominant bands by western blot hybridization whose sizes matched the predicted molecular weights of HOXA13 wild-type (43 kDa) and mutant proteins (64 kDa) (Fig. 3D). The ability of αHoxa13 to immunoprecipitate native HOXA13 was confirmed by western blot analysis of precipitated cell lysates expressing full-length HOXA13 tagged with an HA epitope (Fig. 3E). In cultured limb mesenchyme, the *Hoxa13* antibody co-localizes with endogenous HOXA13-GFP, confirming the specificity of the *Hoxa13* antibody (Fig. 3F-I).

Next, to verify that endogenous HOXA13 binds the same *Bmp2* and *Bmp7* enhancer elements in the developing limb, αHoxa13 was used to immunoprecipitate chromatin from wild-type and homozygous mutant limbs. In wild-type limbs, chromatin immunoprecipitated with αHoxa13 consistently contained the enhancer elements bearing the *Bmp2C1*, *C3* and

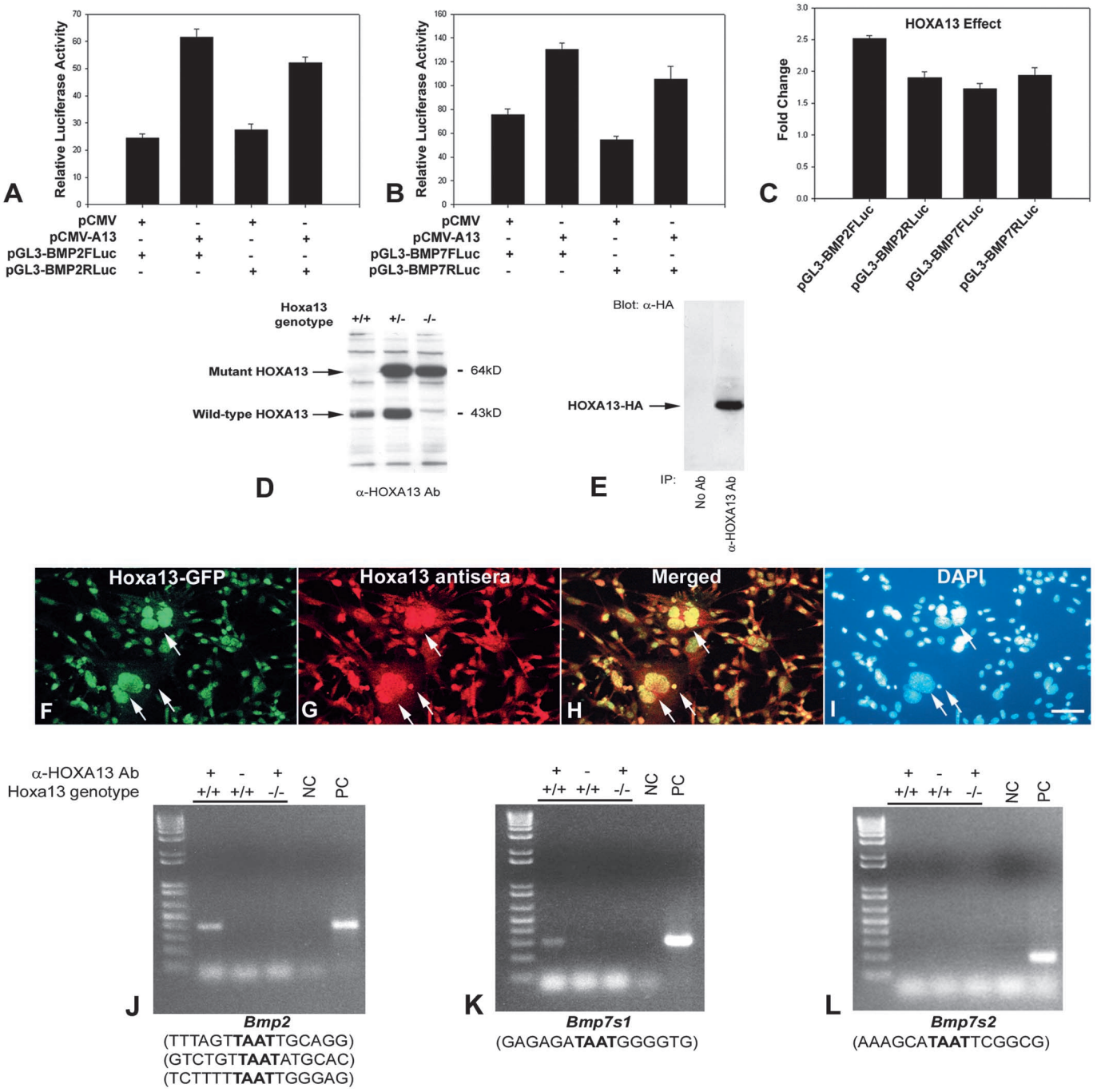

Fig. 3. HOXA13 activates transcription from the *Bmp2* and *Bmp7* enhancer regions, and associates with these enhancers in vivo. Co-transfection of NG108-15 cells with luciferase reporter plasmids containing forward or reverse orientations of the *Bmp2* enhancer sequence (A,C), or the *Bmp7* enhancer sequence (B,C), and pCMV-A13 resulted in 2.5- and 1.8-fold (*Bmp2*), and 1.8- and 2.0-fold (*Bmp7*), increases in RLA, when compared with identical transfections with the control pCMV vector. Luciferase activity was normalized for transfection efficiency using a Renilla Luciferase control plasmid in all co-transfection assays. Bars represent the standard deviation of results derived from four transfection assays. (D) Western blot analysis of protein lysates derived from *Hoxa13* wild-type (+/+), heterozygous mutant (+/–) and homozygous mutant (–/–) tissues confirms that the *Hoxa13* antibody recognizes proteins of the correct molecular weight for wild-type HOXA13 (43 kDa) and mutant HOXA13-GFP (64 kDa). (E) The *Hoxa13* antibody immunoprecipitates HA-tagged full-length HOXA13. (F-I) Immunostaining of cultured limb mesenchyme from HOXA13-GFP mutant mice, using the *Hoxa13* antibody, reveals strong nuclear co-localization (H, yellow, arrows) between the endogenous HOXA13-GFP protein (F) and the *Hoxa13* antibody (G,H). Nuclei are stained with DAPI (I). (J-L) Chromatin immunoprecipitation using the *Hoxa13* antibody confirms that wild-type (+/+) HOXA13 binds the *Bmp2* (J) and *Bmp7s1* (K) enhancer regions in the developing limb, whereas immunoprecipitates from mutant limbs (–/–) lacking the HOXA13 DNA-binding domain did not contain the *Bmp2* and *Bmp7s1* enhancer regions. (L) The absence of *Bmp7s2* sequences in wild-type immunoprecipitates confirms HOXA13 specificity for the TAAT-containing sequences in *Bmp2* and *Bmp7s1*. The TAAT-containing sequences present in the *Bmp2*, *Bmp7s1* and *Bmp7s2* regions are listed below panels J, K, and L. NC, negative PCR control; PC, positive PCR control.

C4, and *Bmp7s1* nucleotide sequences (Fig. 3J,K). By contrast, chromatin immunoprecipitations from *Hoxa13* homozygous mutant limbs did not contain these same enhancer regions, which is consistent with the ablation of the DNA-binding domain in the *Hoxa13*^{GFP} mutant allele (Stadler et al., 2001) (Fig. 3J,K).

To confirm the in vivo specificity of HOXA13 for the TAAT-containing sequences in the *Bmp2* and *Bmp7* enhancers, wild-type αHoxa13 chromatin immunoprecipitates were also examined for the presence of the *Bmp7s2* sequence, which contains a TAAT core sequence but is not bound by the A13-DBD peptide (data not shown). In all cases examined, the *Bmp7s2* sequence could not be detected in wild-type chromatin immunoprecipitates, confirming the in vivo specificity of HOXA13 for the *Bmp2* and *Bmp7s1* sequences (Fig. 3L). These results strongly suggest that endogenous HOXA13 directly binds the *Bmp2* and *Bmp7* enhancer sequences, and that it is through these interactions that HOXA13 controls the expression of *Bmp2* and *Bmp7* in the distal limb.

Reduced *Bmp2* and *Bmp7* expression underlies the loss of IPCD in the *Hoxa13* homozygous mutant limb

Recognizing that HOXA13 can regulate gene expression through the *Bmp2* and *Bmp7* enhancer elements in vitro (Fig. 3A-C), and that it associates with these enhancer sites in the developing limb (Fig. 3J,K), we hypothesized that the limb phenotypes exhibited by *Hoxa13* homozygous mutants must be due, in part, to insufficient levels of BMP2 and BMP7. Testing this hypothesis, we examined whether increasing the levels of BMP2 or BMP7 in *Hoxa13* mutant autopods could rescue some aspects of the interdigital or interarticular joint phenotypes. For the interarticular malformations, supplementation of the autopod tissues with BMP2- or BMP7-treated beads could not restore the normal formation of the joint regions (Fig. 1E,F; data not shown). By contrast, supplementation of the interdigital tissues with either BMP2- or BMP7-treated beads restored distal IPCD in *Hoxa13* homozygous mutants, whereas control experiments using PBS-treated beads did not affect the levels of IPCD in either homozygous mutant or heterozygous control limbs (Fig. 4A-F). These results suggest that BMP insufficiency may underlie the loss of IPCD in *Hoxa13* mutant limbs.

However, although exogenous BMP2 or BMP7 can reinitiate IPCD in *Hoxa13* mutant limbs, the levels of IPCD were never equivalent to identical treatments in *Hoxa13* heterozygous limbs (compare Fig. 4A with 4D, and 4B with 4E). This result suggests that the competency of the interdigital tissues to fully respond to BMP signals may also be affected in *Hoxa13* mutant limbs. To test this possibility, we examined whether exogenous treatments with BMP2 or BMP7 induced *Msx2* expression to different degrees in wild-type versus mutant limbs. Exogenous applications of BMP2 or BMP7 induced *Msx2* expression in the tissue immediately surrounding the implanted beads in *Hoxa13* mutant and wild-type limbs, whereas treatments with beads soaked in PBS did not induce *Msx2* expression (Fig. 4G-L). For both BMP2 and BMP7 treatments, the level of *Msx2* induction was consistently lower in the homozygous mutant limbs (Fig. 4H,J), confirming that the interdigital tissues of *Hoxa13* mutants lack the competency to fully transduce BMP signals. This finding suggests that additional components in the BMP-signaling pathway may be affected by loss of HOXA13 function, although no differences in the expression of BMP-receptors *Ia*, *Ib* or *II* were detected between wild-type and *Hoxa13* mutant limbs at E12.5-13.5 (data not shown).

IPCD is delayed in *Bmp7* mutant mice

TUNEL analysis of *Bmp7* mutant limbs at E13.5 revealed a significant delay in IPCD between digits II and III (Fig. 5A-D), which is the same interdigital region lacking IPCD in *Hoxa13* homozygous mutants (Stadler et al., 2001). This result suggests that reductions in BMP7 in *Hoxa13* mutant limbs can affect IPCD initiation, particularly in tissues where responsiveness to BMP signals is also reduced. For the region between digits III and IV, TUNEL-positive cells were detected

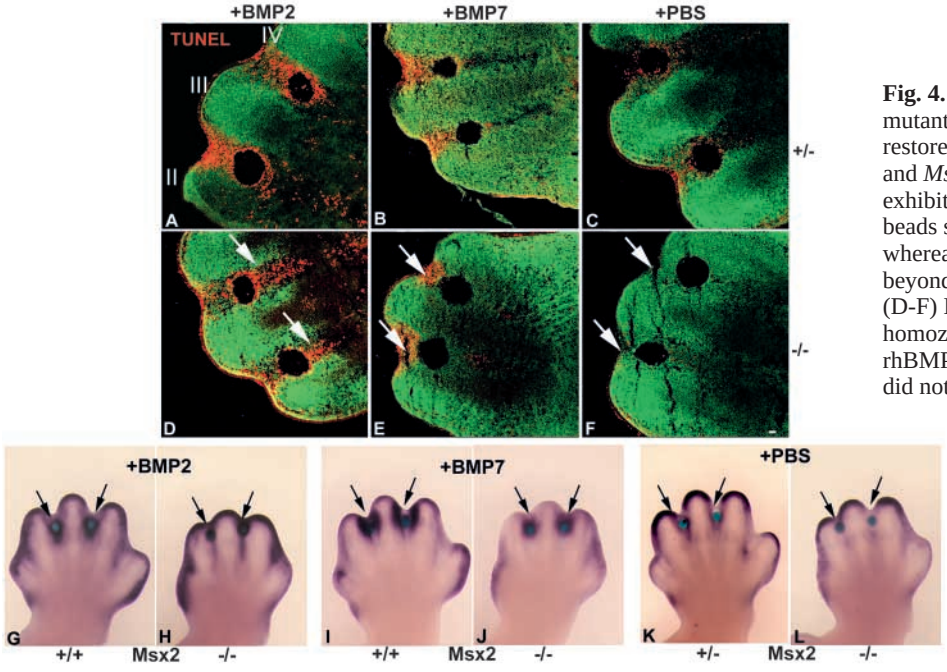

Fig. 4. Supplementation of *Hoxa13* homozygous mutant limbs with BMP2 or BMP7 partially restores interdigital programmed cell death (IPCD) and *Msx2* expression. (A-C) *Hoxa13* heterozygotes exhibited elevated levels of IPCD when treated with beads soaked in 0.1 mg/ml rhBMP2 or rhBMP7, whereas PBS control beads did not elevate IPCD beyond normal levels in organ cultured limbs. (D-F) IPCD is partially restored in *Hoxa13* homozygous mutants in the presence of rhBMP2- or rhBMP7-treated beads, whereas PBS-treated beads did not re-initiate IPCD. Arrows denote sites of IPCD as detected by TUNEL assay (red signal). (G-J) Organ cultures of *Hoxa13* mutant limbs treated with rhBMP2 or rhBMP7 exhibit reduced levels of *Msx2* induction (arrows), when compared with age-matched controls. (K,L) Control treatments using PBS-beads had no affect on *Msx2* expression (arrows). Roman numerals denote digits II, III and IV. Scale bar: 50 μm.

at slightly elevated levels in *Bmp7* mutants, suggesting that BMP7 may regulate IPCD in a differential manner between digits II and III, versus digits III and IV.

HOXA13 functions upstream of *Bmp2* and *Bmp7* in the developing autopod

Previous investigations of BMP function indicate that BMP2 can induce *Hoxa13* expression to control forelimb muscle patterning (Hashimoto et al., 1999). This result led us to examine whether BMP2 or BMP7 may function in a similar manner in the developing mouse autopod. In all cases examined (4/4), supplementation of the interdigital tissues with BMP2 or BMP7 did not induce *Hoxa13* expression (Fig. 5E-G). Furthermore, the elevated levels of *Hoxa13* mRNA in *Hoxa13* mutant autopods (see Fig. 1B,D) supports the conclusion that *Hoxa13* expression is independent of BMP2 and BMP7, as these same tissues exhibit reduced levels of *Bmp2* and *Bmp7* expression (see Fig. 1H,J,L,N).

Discussion

Hoxa13, *Bmp2* and *Bmp7* are co-expressed in the developing autopod mesenchyme

The initial finding of this study is that *Hoxa13* is expressed in specific spatiotemporal domains coincident with *Bmp2* and *Bmp7* expression during embryonic limb development. Further characterization of these expression patterns in *Hoxa13* mutant limbs identified a loss of *Bmp2* and *Bmp7* expression in the distal limb mesenchyme, consistent with the severe defects in IPCD and chondrogenesis exhibited by mutant autopods in these same regions. This characterization places *Hoxa13*, *Bmp2* and *Bmp7* in the same tissues at the same time during normal limb development, and identifies *Bmp2* and *Bmp7* as being reduced in the absence of functional HOXA13.

Hoxa13 coordinates BMP signaling during distal limb development

In the present study one of our major conclusions is that HOXA13 directly regulates the expression of both *Bmp2* and *Bmp7* in the distal autopod. In the absence of HOXA13 function, the interdigital tissues also exhibit reduced responsiveness to BMP-induced programmed cell death. Together these results suggest that HOXA13 functions at multiple levels of the BMP-signaling pathway to direct IPCD and distal digit development. The function of HOX proteins to regulate multiple steps in a developmental pathway is well described in *Drosophila* where Ubx function is required to regulate multiple genes during the specification of wing and haltere structures (Weatherbee et al., 1998). Studies of BMP-receptor function support the conclusion that HOXA13 regulates BMP-signaling to control digit chondrogenesis, as mice lacking BMPR-IB in the distal limb exhibit defects in chondrogenesis remarkably similar to *Hoxa13* mutants (Stadler et al., 2001; Baur et al., 2000; Yokouchi et al., 1995). Similarly, the expression of dominant-negative isoforms of BMPR-IB in chick also affect IPCD, as well as the chondrogenic capacity of the distal limb mesenchyme, phenotypes both described in *Hoxa13* mutant limb mesenchyme (Zou and Niswander, 1996; Zou et al., 1997; Stadler et al., 2001).

In mice, the function of BMP2 during distal limb development is unknown as *Bmp2* homozygous mutants fail to develop to the limb bud stage (Zhang and Bradley, 1996). In *Bmp7* homozygous mutants, the predominant limb phenotype is the addition of an extra anterior digit, whereas the interdigital tissues are completely resolved (Dudley et al., 1995; Luo et al., 1995; Hofmann et al., 1996). The resolution of the interdigital tissues in *Bmp7* mutant mice has been explained by compensatory BMPs co-expressed in these same tissues (Francis-West et al., 1999; Dudley and Robertson, 1997; Dudley et al., 1995; Luo et al., 1995; Lyons et al., 1995; Francis et al., 1994; Hogan et al., 1994; Kingsley, 1994; Lyons et al., 1989). In the limb, IPCD can be stimulated by BMP2, BMP4 and BMP7 (Guha et al., 2002; Merino et al., 1999a; Gañan et al., 1996; Yokouchi et al., 1996). However, in *Bmp7* mutants, the delay in IPCD at E13.5 provides strong evidence that compensatory factors, such as BMP2 and BMP4, do not use the same BMP-signaling components as BMP7, suggesting that additional factors like bioavailability, oligomerization or receptor utilization may also regulate the timing of IPCD (Keller et al., 2004; Groppe et al., 2002; Nohe et al., 2002; Bosukonda et al., 2000; Capdevila and Johnson, 1998; Zou et al., 1997; Zou and Niswander, 1996; Lyons et al., 1995). Thus, in *Hoxa13* homozygous mutants, two compounding events

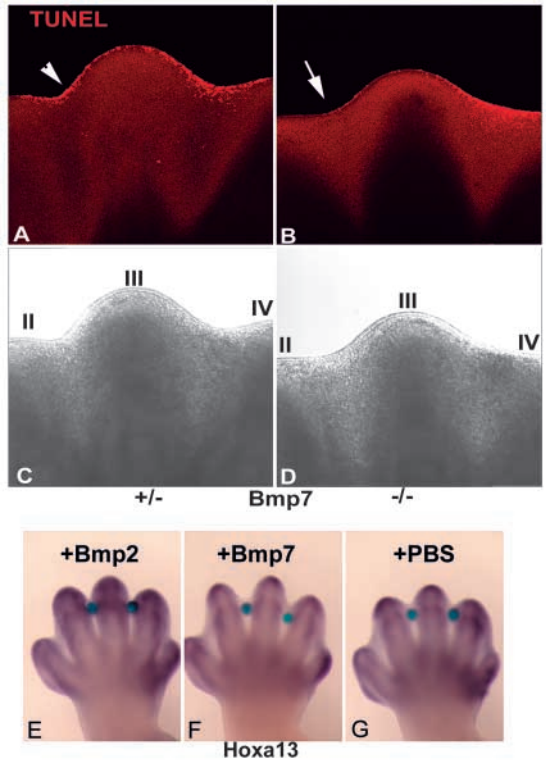

Fig. 5. IPCD is delayed in *Bmp7* homozygous mutant limbs. (A,B) TUNEL analysis of IPCD in E13.5 *Bmp7* mutants (B) revealed a delay in IPCD between digits II and III (arrow), when compared with age-matched heterozygous controls (A, arrowhead). (C,D) Bright-field analysis of the same *Bmp7* heterozygous and mutant limbs shown in A and B. (E-G) Analysis of *Hoxa13* induction by exogenous BMP2 or BMP7. Wild-type limbs treated with 0.1 mg/ml BMP2 (E) or BMP7 (F) did not exhibit any increase in *Hoxa13* expression when compared with PBS controls (G), indicating that in the developing autopod, BMP2 and BMP7 do not regulate *Hoxa13* expression.

contribute to the loss of IPCD. First, BMP2 and BMP7 are reduced in the mutant interdigital tissues to levels below the threshold necessary for IPCD initiation. Second, the competency of the interdigital tissues to respond to BMP signals is affected by loss of *Hoxa13* function.

Surprisingly, mice heterozygous for both *Bmp2* and *Bmp7* (*Bmp2*/*7*) do not exhibit any defects in limb development (Katagiri et al., 1998). This result is most likely explained by compensatory levels of additional BMPs or the upregulation of BMP2, BMP7, or their receptors in *Bmp2*/*7* compound heterozygotes, which to date have not been determined in these mice. Clearly, conditional mutants producing combinatorial losses of redundant BMP proteins will be required to define the functions of these growth factors during distal limb development, particularly in regions where BMPs regulate both digit chondrogenesis and IPCD. Interestingly, the differential use of BMPs to direct digit chondrogenesis may also affect IPCD, as apoptosis in limb mesenchyme is directly linked to the level of chondrogenesis (Omi et al., 2000; Merino et al., 1999b). This finding is consistent with the differential IPCD in *Hoxa13* mutant limbs, where digits II and III exhibit the least amount of chondrogenesis and IPCD (Fig. 1D-F).

Isolation of HOXA13-*Bmp2* and -*Bmp7* enhancer complexes in the developing autopod defines these genes as direct targets of HOXA13 regulation

Using a biochemical approach, we confirmed the C-terminal region of HOXA13 folds into a functional DNA-binding motif and binds DNA in a sequence-specific manner. In vitro, the A13-DBD peptide facilitated the identification of HOXA13-binding sites upstream of *Bmp2* and *Bmp7*. Quantitation of A13-DBD affinity for these enhancer elements revealed a novel series of nucleotide sequences that are preferentially bound with affinities almost 2-fold greater than the DNA regions bound by other homeodomain peptides (Catron et al., 1993).

In vivo, the interactions between HOXA13 and the *Bmp2* and *Bmp7* enhancer regions are conserved, as both enhancer elements were present in immunoprecipitated complexes of HOXA13 bound to DNA. The association of HOXA13 with the *Bmp2* and *Bmp7* enhancer regions in the developing limb strongly suggests that HOXA13 directly regulates the expression of these genes during autopod formation. It is important to note that because chromatin immunoprecipitations do not separate protein complexes prior to immunoprecipitation, we cannot exclude the possibility that HOXA13 interacts with the *Bmp2* and *Bmp7* enhancer regions as part of a protein complex. However, this possibility seems unlikely because of the absence of the *Bmp2* and *Bmp7* enhancer regions in immunoprecipitations using *Hoxa13* mutant limbs that lack the HOXA13 DNA-binding domain, and because of the utilization of these enhancers by full-length HOXA13 to direct gene expression in vitro. In addition, the specificity of HOXA13 DNA-binding is confirmed by the presence of an additional TAAT-containing sequence upstream of *Bmp7* that is not bound by either the A13-DBD peptide (data not shown) or the full-length endogenous HOXA13, as determined by chromatin immunoprecipitation from wild-type autopods (Fig. 3L). This finding confirms that the nucleotides flanking the core TAAT sequence are crucial for HOXA13 binding, supporting our hypothesis that HOXA13 interacts with specific DNA sequences to facilitate its tissue-specific regulation of gene expression (Catron et al., 1993; Pellerin et al., 1994).

Previous investigations of HOXA13 function indicate that *Bmp4* expression may also be regulated by HOXA13 DNA-binding (Suzuki et al., 2003). However, by our analysis, the expression of *Bmp4* appears to be normal in *Hoxa13* mutant limbs (data not shown), suggesting that the cooperative regulation of *Bmp4* by SP1 may compensate for the loss of HOXA13 DNA-binding function. This finding is consistent with the absence of the *Bmp4* sequence in the wild-type limb chromatin immunoprecipitated with a *Hoxa13* antibody (data not shown). In the N terminus of HOXA13, protein-protein interactions may also facilitate some aspects of its function, as mutations expanding the number of N-terminal polyalanine residues cause defects in limb and genitourinary development that are similar to those resulting from mutations ablating the HOXA13 DNA-binding domain (Goodman et al., 2000; Mortlock and Innis, 1997).

In this paper, we present the first evidence that during limb development HOXA13 directly interacts with gene-regulatory elements upstream of *Bmp2* and *Bmp7*. In vivo, the loss of HOXA13 DNA-binding function abolishes interactions with these enhancer elements and reduces the expression of *Bmp2* and *Bmp7* in the developing autopod, causing defects that phenocopy malformations associated with perturbations in BMP signaling. Together, these findings strongly suggest that HOXA13 controls the morphogenesis of discrete autopod tissues by regulating *Bmp2* and *Bmp7* expression through direct interactions with *Bmp2* and *Bmp7* enhancer elements, confirming our hypothesis that the phenotypes exhibited by *Hoxa13* mutant mice reflect a loss in the tissue-specific regulation of direct target genes.

The authors thank Dr Brigid Hogan for the critical reading of this manuscript. This work was supported by research grants from the Shriners Hospital for Children and the National Institutes of Health (H.S.S.), and by a NIH pre-doctoral fellowship (W.M.K.).

References

Baur, S. T., Mai, J. J. and Dymecki, S. M. (2000). Combinatorial signaling through BMP-receptor IB and GDF5: shaping of the distal mouse limb and the genetics of distal limb diversity. *Development* **127**, 605-619.

Bosukonda, D., Shih, M. S., Sampath, K. T. and Vukicevic, S. (2000). Characterization of receptors for osteogenic protein-1/bone morphogenetic protein-7 (OP-1/BMP-7) in rat kidneys. *Kidney Int.* **58**, 1902-1911.

Boulet, A. M. and Capecchi, M. R. (2004). Multiple roles of Hoxa11 and Hoxd11 in the formation of the mammalian forelimb zeugopod. *Development* **131**, 299-309.

Capdevila, J. and Johnson, R. L. (1998). Endogenous and ectopic expression of noggin suggests a conserved mechanism for regulation of BMP function during limb and somite patterning. *Dev. Biol.* **197**, 205-217.

Catron, K. M., Iler, N. and Abate, C. (1993). Nucleotides flanking a conserved TAAT core dictate the DNA-binding specificity of three murine homeodomain proteins. *Mol. Cell. Biol.* **13**, 2354-2365.

Chiang, C., Litingtung, Y., Lee, E., Young, K. E., Corden, J. L., Westphal, H. and Beachy, P. A. (1996). Cyclopia and defective axial patterning in mice lacking Sonic hedgehog gene function. *Nature* **383**, 407-413.

Crossley, P. H., Minowada, G., MacArthur, C. A. and Martin, G. R. (1996). Roles for FGF8 in the induction, initiation, and maintenance of chick limb development. *Cell* **84**, 127-136.

Davis, A. P. and Capecchi, M. R. (1994). Axial homeosis and appendicular skeleton defects in mice with a targeted disruption of hoxd-11. *Development* **120**, 2187-2198.

Davis, A. P., Witte, D. P., Hsieh-Li, H. M., Potter, S. S. and Capecchi, M.

R. (1995). Absence of radius and ulna in mice lacking hoxa-11 and hoxd-11. *Nature* **375**, 791-795.

Dolle, P. and Duboule, D. (1989). Two gene members of the murine HOX-5 complex show regional and cell-type specific expression in developing limbs and gonads. *EMBO J.* **8**, 1507-1515.

Dudley, A. T. and Robertson, E. J. (1997). Overlapping expression domains of bone morphogenetic protein family members potentially account for limited tissue defects in BMP7 deficient embryos. *Dev. Dyn.* **208**, 349-362.

Dudley, A. T., Lyons, K. M. and Robertson, E. J. (1995). A requirement for bone morphogenetic protein-7 during development of the mammalian kidney and eye. *Genes Dev.* **9**, 2795-2807.

Francis, P. H., Richardson, M. K., Brickell, P. M. and Tickle, C. (1994). Bone morphogenetic proteins and a signalling pathway that controls patterning in the developing chick limb. *Development* **120**, 209-218.

Francis-West, P. H., Parish, J., Lee, K. and Archer, C. W. (1999). BMP/GDF-signalling interactions during synovial joint development. *Cell Tissue Res.* **296**, 111-119.

Fromental-Ramain, C., Warot, X., Lakkaraju, S., Favier, B., Haack, H., Birling, C., Dierich, A., Dolle, P. and Chambon, P. (1996a). Specific and redundant functions of the paralogous Hoxa-9 and Hoxd-9 genes in forelimb and axial skeleton patterning. *Development* **122**, 461-472.

Fromental-Ramain, C., Warot, X., Messadecq, N., LeMeur, M., Dolle, P. and Chambon, P. (1996b). Hoxa-13 and Hoxd-13 play a crucial role in the patterning of the limb autopod. *Development* **122**, 2997-3011.

Gañan, Y., Macias, D., Duterque-Coquillaud, M., Ros, M. A. and Hurle, J. M. (1996). Role of TGF betas and BMPs as signals controlling the position of the digits and the areas of interdigital cell death in the developing chick limb autopod. *Development* **122**, 2349-2357.

Goodman, F. R., Bacchelli, C., Brady, A. F., Brueton, L. A., Fryns, J. P., Mortlock, D. P., Innis, J. W., Holmes, L. B., Donnenfeld, A. E., Feingold, M. et al. (2000). Novel HOXA13 mutations and the phenotypic spectrum of hand-foot-genital syndrome. *Am. J. Hum. Genet.* **67**, 197-202.

Grenier, J. K. and Carroll, S. B. (2000). Functional evolution of the Ultrabithorax protein. *Proc. Natl. Acad. Sci. USA* **97**, 704-709.

Groppe, J., Greenwald, J., Wiater, E., Rodriguez-Leon, J., Economides, A. N., Kwiatkowski, W., Affolter, M., Vale, W. W., Belmonte, J. C. and Choe, S. (2002). Structural basis of BMP signalling inhibition by the cystine knot protein Noggin. *Nature* **420**, 636-642.

Guha, U., Gomes, W. A., Kobayashi, T., Pestell, R. G. and Kessler, J. A. (2002). In vivo evidence that BMP signaling is necessary for apoptosis in the mouse limb. *Dev. Biol.* **249**, 108-120.

Gurrieri, F., Kjaer, K. W., Sangiorgi, E. and Neri, G. (2002). Limb anomalies: developmental and evolutionary aspects. *Am. J. Med. Genet.* **115**, 231-244.

Haack, H. P. and Gruss, P. (1993). The establishment of murine Hox-1 expression domains during patterning of the limb. *Dev. Biol.* **157**, 410-422.

Hashimoto, K., Yokouchi, Y., Yamamoto, M. and Kuroiwa, A. (1999). Distinct signaling molecules control Hoxa-11 and Hoxa-13 expression in the muscle precursor and mesenchyme of the chick limb bud. *Development* **126**, 2771-2783.

Hofmann, C., Luo, G., Balling, R. and Karsenty, G. (1996). Analysis of limb patterning in BMP-7-deficient mice. *Dev. Genet.* **19**, 43-50.

Hogan, B. L., Blessing, M., Winnier, G. E., Suzuki, N. and Jones, C. M. (1994). Growth factors in development: the role of TGF-beta related polypeptide signalling molecules in embryogenesis. *Dev. Suppl.* 53-60.

Hombría, J. C. and Lovegrove, B. (2003). Beyond homeosis–HOX function in morphogenesis and organogenesis. *Differentiation* **71**, 461-476.

Katagiri, T., Boorla, S., Frendo, J. L., Hogan, B. L. M. and Karsenty, G. (1998). Skeletal abnormalities in doubly heterozygous Bmp4 and Bmp7 mice. *Dev. Genet.* **22**, 340-348.

Kaufman, M. H. and Bard, J. B. L. (eds) (1999). The Limbs. In *The Anatomical Basis of Mouse Development*, pp. 93-97. San Diego, CA: Academic Press.

Keller, S., Nickel, J., Zhang, J. L., Sebald, W. and Mueller, T. D. (2004). Molecular recognition of BMP-2 and BMP-receptor IA. *Nat. Struc. Mol. Biol.* **11**, 481-488.

Kingsley, D. M. (1994). What do BMPs do in mammals? Clues from the mouse short-ear mutation. *Trends Genet.* **10**, 16-21.

Kmita, M., Fraudeau, N., Herault, Y. and Duboule, D. (2002). Serial deletions and duplications suggest a mechanism for the collinearity of Hoxd genes in limbs. *Nature* **420**, 145-150.

Lewandoski, M., Sun, X. and Martin, G. R. (2000). Fgf8 signalling from the AER is essential for normal limb development. *Nat. Genet.* **26**, 460-463.

Logan, M. (2003). Finger or toe: the molecular basis of limb identity. *Development* **130**, 6401-6410.

Loomis, C. A., Kimmel, R. A., Tong, C. X., Michaud, J. and Joyner, A. L. (1998). Analysis of the genetic pathway leading to formation of ectopic apical ectodermal ridges in mouse Engrailed-1 mutant limbs. *Development* **125**, 1137-1148.

Luo, G., Hofmann, C., Bronckers, A. L., Sohocki, M., Bradley, A. and Karsenty, G. (1995). BMP-7 is an inducer of nephrogenesis, and is also required for eye development and skeletal patterning. *Genes Dev.* **9**, 2808-2820.

Lyons, K. M., Pelton, R. W. and Hogan, B. L. (1989). Patterns of expression of murine Vgr-1 and BMP-2a RNA suggest that transforming growth factor-beta-like genes coordinately regulate aspects of embryonic development. *Genes Dev.* **3**, 1657-1668.

Lyons, K. M., Hogan, B. L. and Robertson, E. J. (1995). Colocalization of BMP 7 and BMP 2 RNAs suggests that these factors cooperatively mediate tissue interactions during murine development. *Mech. Dev.* **50**, 71-83.

Macias, D., Ganan, Y., Sampath, T. K., Piedra, M. E., Ros, M. A. and Hurle, J. M. (1997). Role of BMP-2 and OP-1 (BMP-7) in programmed cell death and skeletogenesis during chick limb development. *Development* **124**, 1109-1117.

Manley, N. R. and Capecchi, M. R. (1995). The role of Hoxa-3 in mouse thymus and thyroid development. *Development* **121**, 1989-2003.

Mariani, F. V. and Martin, G. R. (2003). Deciphering skeletal patterning: clues from the limb. *Nature* **423**, 319-325.

Merino, R., Gañan, Y., Macias, D., Economides, A. N., Sampath, K. T. and Hurle, J. M. (1998). Morphogenesis of digits in the avian limb is controlled by FGFs, TGFbetas, and noggin through BMP signaling. *Dev. Biol.* **200**, 35-45.

Merino, R., Gañan, Y., Macias, D., Rodriguez-Leon, J. and Hurle, J. M. (1999a). Bone morphogenetic proteins regulate interdigital cell death in the avian embryo. *Ann. New York Acad. Sci.* **887**, 120-132.

Merino, R., Rodriguez-Leon, J., Macias, D., Gañan, Y., Economides, A. N. and Hurle, J. M. (1999b). The BMP antagonist Gremlin regulates outgrowth, chondrogenesis, and programmed cell death in the developing limb. *Development* **126**, 5515-5522.

Min, H., Danilenko, D. M., Scully, S. A., Bolon, B., Ring, B. D., Tarpley, J. E., DeRose, M. and Simonet, W. S. (1998). Fgf-10 is required for both limb and lung development and exhibits striking functional similarity to Drosophila branchless. *Genes Dev.* **12**, 3156-3161.

Moon, A. M. and Capecchi, M. R. (2000). Fgf8 is required for outgrowth and patterning of the limbs. *Nat. Genet.* **26**, 455-459.

Morgan, E. A., Nguyen, S. B., Scott, V. and Stadler, H. S. (2003). Loss of Bmp7 and Fgf8 signaling in Hoxa13-mutant mice causes hypospadia. *Development* **130**, 3095-3109.

Mortlock, D. P. and Innis, J. W. (1997). Mutation of HOXA13 in hand-foot-genital syndrome. *Nat. Genet.* **15**, 179-180.

Niswander, L. (2003). Pattern formation: old models out on a limb. *Nat. Rev. Genet.* **4**, 133-143.

Nohe, A., Hassel, S., Ehrlich, M., Neubauer, F., Sebald, W., Henis, Y. I. and Knaus, P. (2002). The mode of bone morphogenetic protein (BMP) receptor oligomerization determines different BMP-2 signaling pathways. *J. Biol. Chem.* **277**, 5330-5338.

Ohuchi, H., Nakagawa, T., Yamamoto, A., Araga, A., Ohata, T., Ishimaru, Y., Yoshioka, H., Kuwana, T., Nohno, T., Yamasaki, M. et al. (1997). The mesenchymal factor, FGF10, initiates and maintains the outgrowth of the chick limb bud through interaction with FGF8, an apical ectodermal factor. *Development* **124**, 2235-2244.

Omi, M., Sato-Maeda, M. and Ide, H. (2000). Role of chondrogenic tissues in programmed cell death and BMP expression in chick limbs. *Int. J. Dev. Biol.* **44**, 381-388.

Parr, B. A. and McMahon, A. P. (1995). Dorsalizing signal Wnt-7a required for normal polarity of D-V and A-P axes of mouse limb. *Nature* **374**, 350-353.

Pellerin, I., Schnabel, C., Catron, K. M. and Abate, C. (1994). Hox proteins have different affinities for a consensus DNA site that correlate with the positions of their genes on the hox cluster. *Mol. Cell. Biol.* **14**, 4532-4545.

Riddle, R. D., Johnson, R. L., Laufer, E. and Tabin, C. (1993). Sonic hedgehog mediates the polarizing activity of the ZPA. *Cell* **75**, 1401-1416.

Sekine, K., Ohuchi, H., Fujiwara, M., Yamasaki, M., Yoshizawa, T., Sato, T., Yagishita, N., Matsui, D., Koga, Y., Itoh, N. et al. (1999). Fgf10 is essential for limb and lung formation. *Nat. Genet.* **21**, 138-141.

Solursh, M., Reiter, R. S., Jensen, K. L., Kato, M. and Bernfield, M. (1990).

Transient expression of a cell surface heparan sulfate proteoglycan (syndecan) during limb development. *Dev. Biol.* **140**, 83-92.

Spitz, F., Gonzalez, F. and Duboule, D. (2003). A global control region defines a chromosomal regulatory landscape containing the HoxD cluster. *Cell* **113**, 405-417.

Stadler, H. S., Higgins, K. M. and Capecchi, M. R. (2001). Loss of Eph-receptor expression correlates with loss of cell adhesion and chondrogenic capacity in Hoxa13 mutant limbs. *Development* **128**, 4177-4188.

Suzuki, M., Ueno, N. and Kuroiwa, A. (2003). Hox proteins functionally cooperate with the GC box-binding protein system through distinct domains. *J. Biol. Chem.* **278**, 30148-30156.

Tickle, C., Shellswell, G., Crawley, A. and Wolpert, L. (1976). Positional signalling by mouse limb polarising region in the chick wing bud. *Nature* **259**, 396-397.

Tickle, C. (2003). Patterning systems – from one end of the limb to the other. *Dev. Cell* **4**, 449-458.

Weatherbee, S. D., Halder, G., Kim, J., Hudson, A. and Carroll, S. (1998). Ultrabithorax regulates genes at several levels of the wing-patterning hierarchy to shape the development of the Drosophila haltere. *Genes Dev.* **12**, 1474-1482.

Wellik, D. M. and Capecchi, M. R. (2003). Hox10 and Hox11 genes are required to globally pattern the mammalian skeleton. *Science* **301**, 363-367.

Yokouchi, Y., Nakazato, S., Yamamoto, M., Goto, Y., Kameda, T., Iba, H. and Kuroiwa, A. (1995). Misexpression of Hoxa-13 induces cartilage homeotic transformation and changes cell adhesiveness in chick limb buds. *Genes Dev.* **9**, 2509-2522.

Yokouchi, Y., Sakiyama, J., Kameda, T., Iba, H., Suzuki, A., Ueno, N. and Kuroiwa, A. (1996). BMP-2/-4 mediate programmed cell death in chicken limb buds. *Development* **122**, 3725-3734.

Zhang, H. and Bradley, A. (1996). Mice deficient for BMP2 are nonviable and have defects in amnion/chorion and cardiac development. *Development* **122**, 2977-2986.

Zou, H. and Niswander, L. (1996). Requirement for BMP signaling in interdigital apoptosis and scale formation. *Science* **272**, 738-741.

Zou, H., Wieser, R., Massague, J. and Niswander, L. (1997). Distinct roles of type I bone morphogenetic protein receptors in the formation and differentiation of cartilage. *Genes Dev.* **11**, 2191-2203.

Zuzarte-Luís, V. and Hurlé, J. M. (2002). Programmed cell death in the developing limb. *Int. J. Dev. Biol.* **46**, 871-876.